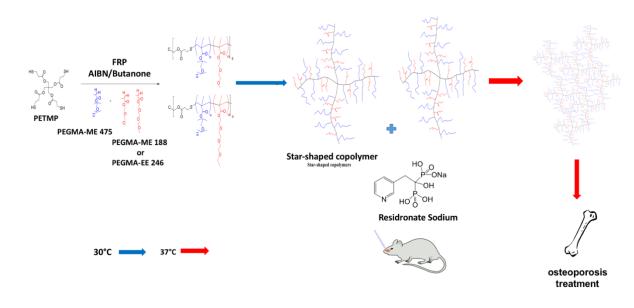# Star-shaped poly(oligoethylene glycol) copolymer-based gels: thermo-responsive behaviour and bioapplicability for risedronate intranasal delivery

Mahmoud E. Soliman[1], Enas Elmowafy[1], Luca Casettari[2] and Cameron Alexander[3]*

[1]Department of Pharmaceutics and Industrial Pharmacy, Faculty of Pharmacy, Ain Shams University, Cairo, Egypt, Monazzamet Elwehda Elafrikeya Street, Abbaseyya, Cairo, Egypt, 11566
[2]Department of Biomolecular Sciences, School of Pharmacy, University of Urbino Carlo Bo, Piazza del Rinascimento, 6, 61029 Urbino (PU), Italy
[3]School of Pharmacy, Boots Science Building, University of Nottingham, University Park, NG7 2RD Nottingham, UK

* Corresponding author:

Luca Casettari,

Associate Professor in Pharmaceutical Technology

University of Urbino

Department of Biomolecular Sciences,

School of Pharmacy,

Piazza Rinascimento, 6, 61029 Urbino (PU), Italy

E-mail: luca.casettari@uniurb.it

33   **Graphical Abstract**

34

35   **Star-shaped poly(oligoethylene glycol) gels for nasal delivery of risedronate**

36

37

38

39

40

41

42

43

44

45

46

47

48

49

50

51

52

53

Abstract

The aim of this work was to obtain an intranasal delivery system with improved mechanical and mucoadhesive properties that could provide prolonged retention time for the delivery of risedronate (RS). For this, novel in situ forming gels comprising thermo-responsive star-shaped polymers, utilizing either polyethylene glycol methyl ether (PEGMA-ME 188, Mn 188) or polyethylene glycol ethyl ether (PEGMA-EE 246, Mn 246), with polyethylene glycol methyl ether (PEGMA-ME 475, Mn 475), were synthesized and characterized. RS was trapped in the selected gel-forming solutions at a concentration of 0.2% w/v. The pH, rheological properties, in vitro drug release, ex vivo permeation as well as mucoadhesion were also examined. MTT assays were conducted to verify nasal tolerability of the developed formulations. Initial in vivo studies were carried out to evaluate anti-osteoporotic activity in a glucocorticoid induced osteoporosis model in rats. The results showed successful development of thermo-sensitive formulations with favorable mechanical properties at 37°C, which formed non-irritant, mucoadhesive porous networks, facilitating nasal RS delivery. Moreover, sustained release of RS, augmented permeability and marked anti-osteoporotic efficacy as compared to intranasal (IN) and intravenous (IV) RS solutions were realized. The combined results show that the in-situ gels should have promising application as nasal drug delivery systems.

Keywords:

1. Introduction

Star-shaped polymers are formed of a core connected to three or more linear chains (arms) with similar lengths (Daoud and Cotton, 1982). They not only have condensed structure with small volume and size compared to linear analogues but also can be decorated with different end groups that make them beneficial in different applications (Dong et al., 2015). Arms of star-shaped polymers may be either homo-, or co-polymers, hence the final properties of the resulting polymers (e.g., star-block and heterostar copolymers) may be adjusted by choosing the respective chemical structure of an arm and core, depending on the required application (Aloorkar et al., 2012).

Among star-shaped polymers, polyethylene oxide (PEO) based polymers have been prepared, tested and characterized for many biomedical, pharmaceutical and tissue engineering applications (Harris, 2013). PEO based star-shaped polymers are non-ionic and biocompatible macromolecules that have high stability and solubility, hence can function to shield drug payloads from inactivation by the immune system (Lapienis, 2009). Moreover, designing polymers to have PEO chains incorporated in star architectures may be advantageous compared to linear PEO counterparts as these materials can have multiple functional groups at chain-ends or in core-components, adding to the applicability of these polymers (Gasteier et al., 2007).

Recently, star-shaped PEO-based polymers have been tested for their thermoresponsive properties (Badi and Lutz, 2009). These polymers were found to have a defined lower critical solution temperature (LCST) in both water and physiological fluids. The thermoresponsive behaviour of these polymers is thought to be due to their amphiphilic nature (hydrophilic oligo(ethylene glycol) side chains and hydrophobic backbones) (Jeong et al., 2012).

The copolymerization of two oligo(ethylene glycol) methacrylates with different chain lengths, namely PEGMA-ME 188 and PEGMA-ME 475 was reported and produced thermoresponsive copolymers with adjustable phase transition temperature values (Saeed et al., 2011). The reversible phase changes of these copolymers were found to be affected by their concentration and chain length as well as ionic strength (Magnusson et al., 2008). Hence, these polymers were suggested as promising candidates for the formulation of thermoresponsive materials. Oligo(ethylene glycol)-based thermoresponsive materials have now been developed in the form of dendrimers, microgels, and added to silica particles, gold particles, block copolymer aggregates, carbon nanotubes, and planar surfaces (Lutz, 2011).

Hydrogels were used for different applications in drug and cell delivery as well as in tissue engineering as polymer scaffold (Cespi et al., 2014; Caló and Khutoryanskiy, 2015). In situ gelling hydrogels have been exploited for drug delivery through various administration routes and presented a great interest for nasal delivery (Cai et al., 2011; Galgatte et al., 2014; Wavikar et al., 2017).

Osteoporosis and Paget's disease of bone are major problems in women and geriatric patients (Riggs and Melton, 1995). In this regard, various pharmacological molecules have been attempted to accelerate new bone formation such as recombinant human fibroblast growth factor-2, thrombin-related peptide, bone morphogenetic protein-2 and bisphosphonates (Hirabayashi and Fujisaki, 2003). Bisphosphonates, as pyrophosphate analogues, possesses a known affinity for bone tissue and an outstanding antiresorptive and osteoclast inhibitory potential (Czuryszkiewicz et al., 2005). These types of drugs are effective in the treatment of Paget's disease, osteoporosis, multiple myeloma, bone metastases, fibrous dysplasia of bone, and breast cancer (Czuryszkiewicz et al., 2005; Nancollas et al., 2006). Nitrogen containing bisphosphonates (e.g. Risedronate (RS)) are many times more potent than the non-nitrogen ones. Despite the interest in fabricating RS carrier platforms, its high polarity and hydrophilicity lead to very poor oral bioavailability ($< 1\%$). In addition, RS exacerbates serious side effects in the gastrointestinal tract (GIT) such as oesophagitis, ulcers and gastritis. Various administration routes for RS, including intravenous, subcutaneous and intramuscular routes, have been attempted in order to improve its poor oral bioavailability ($< 1\%$) and therapeutic efficacy as well as minimizing its side effects (Salzano et al., 2011). Following intravenous (IV) administration, calcium complexes in the blood are formed resulting in possible occurrence of renal failure (Toussaint et al., 2009). Furthermore, injection of sodium salts was reported to develop pain and tissue necrosis at the injection site. Accordingly, a focus of current research is localized delivery of RS via nasal and pulmonary routes (Fazil et al., 2016; Nasr et al., 2011).

In the present work, polymers of star-shaped PEGMA-ME 188 or PEGMA-EE 246 with and without PEGMA-ME 475 were synthesized and characterized for preparing thermoresponsive hydrogels. We aimed to investigate the utilization of the prepared platforms with PEGMA-ME 188 or the PEGMA-EE 246 -co- PEGMA-ME 475 as bio-applicable thermogels with optimal thermoresponsive and mucoadhesive properties in physiological conditions for the nasal delivery of RS. To our knowledge, this is the first study to demonstrate star-shaped poly(oligoethylene

glycol) copolymers in situ gels as nasal delivery carriers for RS and to evaluate their *in vivo* efficacy for the treatment of osteoporosis in rat models.

2. Experimental

2.1. Materials

All solvents and reagents were of analytical or HPLC grade and purchased from Sigma Aldrich (UK) or Fisher Scientific (UK) unless otherwise stated. Deuterated solvents were from Sigma Aldrich (UK) or Cambridge Isotopes (UK). Monomers used in this study (Polyethylene glycol methyl ether (PEGMA-ME 188, Mn 188), polyethylene glycol ethyl ether (PEGMA-EE 246, Mn 246), and polyethylene glycol methyl ether (PEGMA-ME475, Mn 475) were purchased from Sigma Aldrich (UK) and purified before use by passing through a column filled with neutral alumina. 2,2- azobisisobutyronitrile (AIBN) was purchased from Sigma Aldrich (UK) then recrystallized from methanol. Pentaerythritol Tetra (3-mercaptopropionate) (PETMP) and 2-butanone were used as received from Sigma Aldrich (UK). Risedronate sodium was kindly supplied by SPIC Pharma (India). Spectra/Por dialysis membrane, 12,000–14,000 molecular weight cutoff, was purchased from Spectrum Laboratories (Canada). MTT (3-(4,5-dimethylthiazol-2-yl)-2,5-diphenyl-tetrazolium bromide), HEPES buffer, gentamycin, dimethylsulfoxide and sodium lauryl sulphate (SLS) from Sigma-Aldrich (UK). Foetal calf serum, Minimum Essential Medium (MEM), from Lonza (Belgium); and L-glutamine GIBCO®, were purchased from Thermo Fisher Scientific (USA).

2.2 Polymer synthesis and telomerization kinetics

Polymers were prepared by free radical polymerization (Fig. S1). Monomers were weighed into a round bottom flask then PETMP and 20 ml of 2-butanone were added. Lastly AIBN was added and the mixture was degassed with nitrogen for 25 minutes. Then the solution temperature was elevated to 70 °C and polymerization was allowed to proceed at that temperature for 2 h. The reaction was then stopped by cooling the reaction vessel in liquid nitrogen. The polymer was purified from excess monomers and reagents by precipitation three times in hexane.

171 Telemerization kinetics of Poly(PEGMA188-ME) and Poly(PEGMA246-EE) were examined by

172 following the concentrations of monomers and telogen (PETMP) throughout the reaction. Samples

173 were collected at 0, 30, 45, 60, 90, 120, 150 and 180 min and the reaction was stopped by cooling

174 them in ice.

175 Samples were evaluated by ^{1}H-NMR in CDCl$_3$ to detect monomer PEGMA188 for

176 Poly(PEGMA188-ME) and PEGMA246-EE for Poly(PEGMA246-EE) conversion by comparing

177 the integration of monomer vinylic protons to polymer methine protons. The remaining sample

178 was precipitated in hexane then filtered and the filtrate was evaporated under vacuum. The residue

179 left after evaporation was dissolved in water then any PETMP left was determined by iodine

180 titration to determine telogen conversion (Loubat and Boutevin, 2001).

181

182 **2.3 Characterization of the synthesized polymers**

183 **2.3.1 FTIR characterization**

184 FTIR spectra of the polymers were recorded in the range of 4000-400 cm^{-1} on a Nicolet 6700 FTIR

185 (Thermo Scientific, USA), equipped with an attenuated total reflectance (ATR) accessory

186 providing an analysis of the sample surface. Polymeric samples were loaded on KBr discs without

187 previous treatments or special preparation techniques. All spectra were recorded at ambient

188 temperature under vacuum to remove air humidity contribution at a resolution of 4 cm^{-1} and 16

189 scans were recorded for each measurement to obtain an adequate signal to-noise ratio.

190

191 **2.3.2 Nuclear Magnetic Resonance Analysis (^{1}H-NMR)**

192 ^{1}H-NMR spectra were recorded on a Bruker 400 spectrometer (Bruker Avance III, Switzerland) at

193 399.8 MHz (^{1}H) in chloroform-d solutions. All chemical shifts are reported in ppm relative to

194 TMS.

195

196 **2.3.3. Gel Permeation Chromatography (GPC)**

197 As shown in Table 1, the number average molecular weight (M_n), weight average molecular weight

198 (M_w) and polydispersity index (M_w/M_n) of the synthesised polymers were determined using gel

permeation chromatography device (PL-50 PolymerLabs, UK) equipped with refractive index detector. The device columns (30 cm PLgel Mixed- C, 2 in series) were eluted with chloroform and calibrated with polystyrene standards (Mw=162–371100Da) (PolymerLabs, UK).

Standard calibrations as well as analysed samples were maintained at 40°C during analysis and a flow rate of eluent was set at 1ml/min for all experiments. All samples were dissolved in HPLC grade chloroform and filtered using 0.2 μm filter before injecting 100 μL aliquots.

2.3.4. Rheometrical characterizations

The rheological measurements were performed using Physica Rheometer (Anton Paar, USA), equipped with parallel plate geometry (25 mm diameter) and the gap distance between two plates was set as 0.5mm. RheoPlus Software (Version 3.6x) was used for measuring data.

Temperature Ramp experiments were recorded at 0.05% strain at a frequency = 1 rad s^{-1} with a heating rate of 1°C/ min from 10 to 40°C. Before running the experiment, the lower plate and the PP25 were left in contact for 5 min at 10°C. Afterwards, 300 μl of sample was applied on the lower plate. The sample was equilibrated at the desired temperature (10°C) for 4 min before starting the run. The tests have been performed using a fresh aliquot of sample.

2.3.5. UV/ Visible spectroscopy (Temperature dependent turbidity) measurement

A DU 800 UV spectrophotometer (Beckman Coulter, USA) with a thermostat was used for measuring the change in absorption of polymeric sample solutions over a temperature range of 10–50 °C at a wavelength of 550.0 nm. The temperature was controlled and measured using a Peltier plate heating system (Beckman Coulter, USA) and was increased at a rate of 1 °C/min.

2.4. Scanning Electron Microscopy (SEM)

Gel surface morphologies were imaged via SEM. Samples were prepared by spreading freeze dried gels (Poly(PEGMA188-ME-co-PEGMA475-ME) and Poly(PEGMA246-EE-co-PEGMA475-ME)) on an aluminium stub coated with carbon tape. Samples were then coated with a thin layer of gold (Blazer SCD 030 Sputter coater, Blazer Union Ltd, Liechtenstein) for 3 minutes, then images were recorded using a JEOL 6060V scanning electron microscope (JEOL Ltd, UK) at an accelerating voltage of 30kV.

2.5. Incorporation of RS in thermoresponsive gels and pH determination

All the co-polymers used in this study were prepared in cold ultrapure water (15-30% w/w), gels for nasal delivery were prepared to contain 5% mannitol as a tonicity adjuster. The solutions were kept in a refrigerator for at least 24 h to ensure complete dissolution and formation of clear homogeneous solutions. The model hydrophilic drug, RS, at a concentration of 0.2% w/v was then incorporated in the prepared solutions by simple mixing.

The developed formulations were evaluated for pH by using a pH meter (Model 3510, Jenway, UK).

2.6. Viscosity determination of RS loaded thermoresponsive gels

The sol–gel transition behavior of the hydrogels was further evaluated by viscosity measurements. The viscosity of the instilled formulation into the nose is considered to be very important for determination of nasal residence times of drugs. The prepared formulations were allowed to gel at physiological temperature and then the viscosity was determined by a DV-E Viscometer (Brookfield Engineering Laboratories, USA) using spindle no 52 at speeds ranging from 0.5 to 100 rpm (shear rates 1 to 200 sec^{-1}) and over 10% torque. By plotting rheograms of viscosity values versus shear rate, the flow pattern was checked.

2.7 Bioadhesion Strength of RS loaded thermoresponsive gels

To quantify mucin-polymer mucoadhesive strength of gel formulation, a simple viscometric method was used as previously described by (Hassan and Gallo, 1990). The viscosities of 15% (w/v) porcine gastric mucin dispersions in normal saline, co-polymer solutions and mucin–hydrogels (RS loaded Poly(PEGMA188-ME-co-PEGMA475-ME) gel (F2) and RS loaded Poly(PEGMA246-EE-co-PEGMA475-ME) gel (F4)) mixtures were measured at 37 °C using Brookfield viscometer.

The viscosity coefficient was then determined by equation 1:

$$\eta_t = \eta_m + \eta_p + \eta_b \qquad (1)$$

9

258 Where η_t is the viscosity coefficient of the system, η_m and η_p are the individual viscosity

259 coefficients of mucin and polymers, respectively, and η_b is the viscosity component due to the

260 mucoadhesion.

261

262 **2.8 In vitro drug release study**

263 The freshly prepared RS loaded hydrogels were used in in vitro release study similar to the one

264 attempted by (Nasr et al., 2013). In details, hydrogels equivalent to 2 mg RS were loaded in

265 cylinders of cellulose acetate membrane and placed in 15 mL vials containing 7.5 ml physiological

266 normal saline (Wu et al., 2007) maintained at 37 °C in shaker water bath (Kottermann GmbH,

267 Uetze/Hanigsen, Germany) at 50 rpm. As a control, the release of 2 mg RS solution was also

268 performed. At selected time intervals (1, 2, 4, 6, 8, 24, and 48 h), 0.5 mL was sampled from vials

269 and replaced with an equal volume of fresh pre-warmed saline.

270 The quantity of RS released was determined using UV spectrophotometry (UV-Vis

271 spectrophotometer, UV-1601PC, Shimadzu, Japan) at 262 nm. The results of the release

272 experiments are shown as cumulative drug percentage released plotted as a function of time.

273 The release profiles was compared using similarity factor (f_2) according to (Moore, 1996)

274 independent mathematical approach The similarity factor (f_2) was calculated according to equation

275 2:

276 $$f2 = 50 log \left\{ \left[1 + \left(\frac{1}{n} \right) \sum_{t=1}^{n} (Rt - Tt)^2 \right]^{-0.5} \times 100 \right\} \qquad (2)$$

277

278 where n is the number of time points, Rt and Tt are the percent drug released from F2 and F4 at

279 time t. f_2 value between 50 and 100 indicate that the release profiles are similar.

280

281 **2.9 Ex vivo permeation**

282 An ex-vivo nasal permeation study was performed in order to evaluate nasal absorption of RS from

283 the prepared hydrogels. The study was performed by introducing 100 µL of the prepared

284 formulations in the donor compartment of a Franz-type static glass diffusion cell (Variomag

285 Telesystem, H + P Labortechnik, Germany) with a 7.5 mL receptor volume and diffusion surface

286 area: 1.77 cm^2. The hydrogels were placed on a freshly separated sheep nasal mucosa, positioned

287 between the donor and receptor compartments. The receptor compartment was filled with

288 physiological saline (0.9 %, w/w), maintained at 37 ± 0.5 °C. Samples (0.5 ml) were withdrawn

289   from the receptor fluid at appropriate time intervals up to 48 h, and replaced with 0.5 ml of fresh

290   saline. The results of permeation studies are represented as cumulative drug amount (µg)

291   permeated per unit of surface area (cm^2) versus time. The steady state flux (J, $\mu g/cm^2/h$) was

292   determined from the slope of the linear profiles.

293

294   **2.10 In vivo study**

295   In the current study, we tried to evaluate role of RS in osteoporosis model induced by

296   dexamethasone sodium phosphate. All study procedures were evaluated and approved by the

297   Research Ethics Committee of the Faculty of Pharmacy, Ain Shams University. A total of 24

298   female Albino rats weighing 225 to 250 g were selected for this study. Animals were housed under

299   controlled environmental conditions and were maintained in plastic cages with free access to food

300   and water and were kept at a constant temperature of 20-24°C with 12 h light/dark cycle.

301

302   **2.10.1 Glucocorticoid induced osteoporosis model in rats**

303   Following 7 days of acclimatization, glucocorticoid-induced osteoporosis (GIO) was induced in

304   female Albino rats by subcutaneous (SC) administration of Fortecortin® (dexamethasone sodium

305   phosphate) at 8 mg/kg body weight per 7 days for 4 weeks (Fazil et al., 2016). Weights of rats

306   were observed during induction of osteoporosis and their treatment.

307

308   **2.10.2 Animal groups**

309   The rats were divided into six groups (each group contained 4 rats) as follows:

310   Group I (S): Received 30 µl intranasal (IN) normal saline (S) through micropipette attached to a

311   polyethylene tube (negative control group). Group II (DEX): was given subcutaneous (SC)

312   dexamethasone sodium phosphate (DEX) by above mentioned dose (toxic control group). Group

313   III (DEX+ IN RS): was given DEX plus receiving IN RS solution (1mg/kg) (Fujita et al., 2011).

314   Group IV (DEX+ IV RS): was given DEX plus receiving IV RS solution (1mg/kg). Group V

315   (DEX+ IN F2): was given DEX plus receiving IN F2 in situ thermoresponsive gel (volume

316   equivalent to RS 1mg/kg). Group VI (DEX+ IN F4): was given DEX plus receiving IN F4 in situ

317   thermoresponsive gel (volume equivalent to RS 1mg/kg).

318

319   **2.10.3 Biochemical analysis of bone turnover markers**

320 At the end of the study (28 days), animals were killed under general anaesthesia with diethyl ether
321 after blood collection from retro orbital plexus. Blood was centrifuged at 5000 rpm for 10 min and
322 serum stored immediately at -20°C for analysis. Serum alkaline phosphatase, serum calcium level,
323 serum inorganic phosphorus level and serum creatinine were estimated. The values of blood
324 biochemistry were measured in Ain Shams Laboratory Center, Cairo, Egypt using Roche
325 biochemical regeants via photometric assay (Hitachi 917 autoanalyzer, Roche Diagnostics, USA)

326

2.10.4 Histological study of bone internal structure

328 Autopsy samples were taken from the femur bone of rats in different groups and fixed in 10%
329 formal saline for twenty-four hours then decalcification in formic acid. Washing was done with
330 water then alcohol was used for dehydration. Specimens were cleared in xylene and embedded in
331 paraffin wax melted at 56°C in an oven for twenty-four hours. Paraffin tissue blocks were prepared
332 for sectioning at 4 microns thickness by a sledge microtome (Rotary Leica RM2245,USA). The
333 obtained tissue sections were collected on glass slides, deparaffinised, stained by hematoxylin &
334 eosin stain for examination via microscopy (Axiostar Plus, Zeiss, USA) (Banchroft 1996).

335

2.11 Evaluation of nasal cytocompatability

337 MTT assays were used to evaluate the *in vitro* cytotoxicity of the prepared gels on Calu-3 cells.
338 Briefly, cells were seeded at a density of 1×10^4 cells/well in 96-well plates and incubated at 37 °C
339 in a humidified atmosphere (95% RH) with 5% v/v CO_2 (Humid CO_2 incubator, Shel lab 2406,
340 USA). Seven aliquots of the co-polymers solutions (7.81-15.62-31.25-62.5-125-250-500 μg/mL)
341 were added to the wells, followed by incubation for another 24 h. Both sodium dodecyl sulphate
342 treated and untreated cells were used as positive and negative controls respectively. After 24 h of
343 incubation, 20μL of MTT solution (5 mg/mL in phosphate buffered saline pH 7.4 was added to
344 each well and incubated at 37°C for 4 h. then, MTT solution was removed and DMSO was added
345 to solubilize the formed formazan. The absorbance was read at 570 nm on a microplate reader
346 (Tecan Sunrise®, Switzerland). Cell metabolic activity as a proxy for viability (%) was calculated
347 according equation 3:

348

349   Cell metabolic activity (viability, %) = (Absorbance test/Absorbance control) X 100   (3)

350 Where the absorbance control was the absorbance of untreated cells in the control wells.

351

2.12 Statistical analysis

357

3. Results and discussions

3.1. Preparation of gel components and telomerization kinetics

Thermoresponsive polymers were synthesised by free radical polymerization using PETMP as a chain transfer agent. PETMP was chosen as the transfer agent in order to produce star-shaped polymers. The homopolymers of PEGMA-ME 188 and PEGMA-EE246 were prepared as controls to establish telomerisation kinetics before being copolymerized with the more hydrophilic monomer PEGMA-ME475 to adjust the gelation temperature to a value > 30°C (Fig. S2 and Table 1).

The PEGMA based polymers were prepared aiming to combine the advantageous properties of polyethylene glycol (non-toxic, non-immunogenic) and thermosensitivity in one macromolecule. Table 1 demonstrates the molar masses and characteristics of the homo- and co-polymers.

Table 1. Summary of the polymers synthesized in this study

Polymer structure	Mn (kDa)	PDI	Tc (°C)	PEGMA475 (%)	C_T
Poly(PEGMA188-ME)	38.9	1.9	26	0	0.97
Poly(PEGMA188-ME-co-PEGMA475- ME)	36.2	2.1	32	16	---
Poly(PEGMA246-EE)	35	2.3	25	0	0.93
Poly(PEGMA246-EE-co-PEGMA475-ME)	43	2.2	31	10	---

The control of polymer architecture through the use of polyfunctional chain transfer agent in free radical polymerization was investigated, both theoretically and experimentally. Yuan et al studied the telomerization of methyl methacrylate with the tetrafunctional transfer agent PETTMP and found a C_T to be 0.64 (Yuan and Di Silvestro, 1995). It is assumed that the smaller the value of transfer constant ($C_T \approx 1$) is an indication of telomerization reaction efficiency (Loubat and Boutevin, 2001; Pardal et al., 2009).

There are several methods of determining the transfer constant (C_T) of the transfer agent. The most widely used one is given by (O'Brien and Gornick, 1955). This method requires a plot of $\ln[T_0]/[T]$ versus $\ln [M_0]/[M]$ where $[T_0]$, $[T]$, $[M_0]$ and $[M]$ are the molar concentrations of telogen and monomer at time 0 and time t respectively where the value of C_T can be determined from the slope of the line obtained.

This method was applied to the telomerization of PEGMA188-ME and PEGMA246-EE in the presence of PETTMP as a telogen under nitrogen, in 2-butanone at 70 °C, in the presence of AIBN as initiator. Each reaction was monitored by sampling, and each aliquot was quenched in ice to stop the reaction. The monomer (M) and telogen (T) conversions were determined, respectively, with ^{1}H NMR and iodine titration as explained in the experimental section.

From the change of each monomer and telogen concentration in the course of their telomerization, the C_T values were determined for Poly(PEGMA188-ME) and Poly(PEGMA246-EE) and found to be 0.97 and 0.93 respectively, indicating efficient telomerization reaction (Fig. S2).

3.3 Polymer characterization

The chemical structure of copolymers was characterized by FTIR, ^{1}H-NMR, and GPC.

3.3.1 FTIR

14

In order to confirm the formation of the polymers, FTIR spectra were performed as shown in Fig. S3. In the generated spectra, the bands of 1726 and 1113 cm^{-1} were respectively assigned to the C=O and C-O stretching vibrations for carbonyl group of carboxylic ester, the wide band around 3423 cm^{-1} to the O-H stretching vibration, the bands of 2871 cm^{-1} and 1470 to 1380 cm^{-1} to the stretching and bending vibrations of methylene (-CH$_2$). The absence of the acrylate group at the range of 1620 - 1650 cm-1 indicates that acrylate groups were depleted and hence, the successful formation of polymers by free radical polymerisation (Lee et al., 2003).

3.3.2 NMR

The polymers were characterised by NMR spectroscopy as shown in Fig. S4.

^{1}H NMR spectra were recorded in CDCl$_3$ using Bruker 400 MHz. The molar fraction of PEGMA475-ME in Poly(PEGMA246-EE-co-PEGMA475-ME) was calculated from ^{1}H NMR spectra by comparing the overall integration of the methoxy protons (3.41 ppm) to the integration at 1.23 ppm for the 3 terminal protons of ethoxy moiety of PEGMA246-EE.

Poly(PEGMA188-ME) and Poly(PEGMA188-ME-co-PEGMA475-ME)

^{1}H NMR (400 MHz, CDCl$_3$, δ, ppm): 4.25 (-CO-O**CH$_2$**CH$_2$), 4.1-4.2 (C**CH$_2$**OCOCH$_2$-), 3.5-3.75 (-CH$_2$O**CH$_2$CH$_2$**O-), 3.35-3.41 (**CH$_3$**O-), 2.3-2.5 (OCO**CH$_2$**CH$_2$S-), 1.7-2.01 (-S**CH$_2$**C(CH$_3$)-), 0.72-1.16 (-CH$_2$C**(CH$_3$)**-).

Poly(PEGMA246-EE)

^{1}H NMR (400 MHz, CDCl$_3$, δ, ppm): 4.22 (-CO-O**CH$_2$**CH$_2$), 4.1 (C**CH$_2$**OCOCH$_2$-), 3.5-3.7 (-CH$_2$O**CH$_2$CH$_2$**O-), 3.4 (CH$_3$**CH$_2$**O-), 2.2 (OCO**CH$_2$**CH$_2$S-), 1.62-2.06 (-S**CH$_2$**C (CH$_3$)-), 1.23 (**CH$_3$**CH$_2$O-),0.72-1.16 (-CH$_2$C **(CH$_3$)**-).

Poly(PEGMA246-EE-co-PEGMA475-ME)

^{1}H NMR (400 MHz, CDCl$_3$, δ, ppm): 4.3 (-CO-O**CH$_2$**CH$_2$), 4.1 (C**CH$_2$**OCOCH$_2$-), 3.5-3.7 (-CH$_2$O**CH$_2$CH$_2$**O-), 3.47 (CH$_3$**CH$_2$**O-), 3.41 (**CH$_3$**O-), 2.3-2.45 (OCO**CH$_2$**CH$_2$S-), 1.62-2.06 (-S**CH$_2$**C (CH$_3$)-), 1.23 (**CH$_3$**CH$_2$O-), 0.72-1.16 (-CH$_2$C**(CH$_3$)**-).

3.3.3 Gel permeation chromatography (GPC)

Fig. S5 and Table 1 present the molar masses relative to polystyrene standards for the respective polymers. The polymers synthesised had a large polydispersity index, as expected for polymers prepared by free radical polymerization methods. Conventional free radical methods were used since they do not require complex conditions or metals, employed in controlled polymerisations that might be difficult to eliminate and which could otherwise present a source of toxicity (Johnson et al., 2008) when used with cells (Chen et al., 2006). Prior reports have shown that high polydispersity polymers can still form thermogelling solutions (Lietor-Santos et al., 2009).

3.6. Rheological property

Gels made from the prepared polymers were characterised by experiments to measure their elastic/storage ($G`$) and the viscous ($G``$) moduli. The variation of $G`$ with temperature was apparent in temperature/gel moduli plots of a representative gel (Fig. S6A). This could confirm the high dependency of intermolecular attraction between polymer chains, and hence the gel elasticity, on temperature. Below the Lower Critical Solution Temperature (LCST) of the polymers (as estimated from the cloud point), they behaved as viscous fluids with $G`` > G`$. At temperature values around the LCST, a crossover occurred, with $G` > G``$, indicative of gel formation. Both moduli increased with temperature, with $G`$ remaining higher than $G``$.

The ability to manipulate the properties of the gel by changing the thermoresponsive polymer is shown in Fig. S6B. For equivalent composition ratios, gels formed above LCST using homopolymers were of higher moduli than copolymers containing PEGMA475. The rheology experiments thus indicated that the mechanical properties of the gels were able to be tuned by composition, suggesting a simple way of tailoring the gel properties for a particular application.
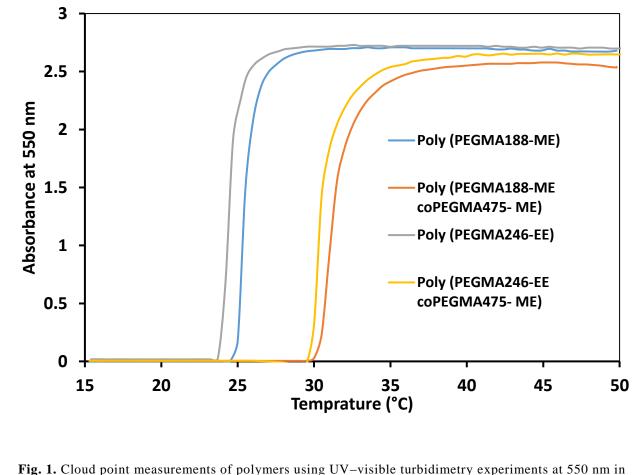
3.3.4. Cloud point determination

Thermoresponsive polymers undergo a coil-to-globule transition at the lower critical solution temperature (LCST) and become water insoluble (Liu et al., 2009). When the polymers are in the collapsed state their solution becomes turbid as a result of polymer chain aggregation.

The solution turbidity starts at the cloud point temperature (Cpt) and this can be easily determined experimentally by light transmission measurement. Cloud point temperatures were measured to estimate the LCST for each polymer (Alava and Saunders, 2006) as shown in table 1.

Phase transitions temperatures of the polymers were modulated by copolymerization of hydrophobic OEGMA component with the hydrophilic PEGMA monomer (Table 1, Fig. 1). We were interested in polymers that would exhibit phase transitions at, or close to, body temperature. it was found that the statistical FRP copolymer of OEGGMA-co-PEGMA (95/5 monomer-feed ratio) met this criterion. As expected, the cloud point temperatures were higher for PEGMA-ME475 copolymers than homopolymers, owing to the presence of hydrophilic monomer. PEGMA-ME475 had the effect of facilitating polymer chain dehydration to happen at higher cloud point value. Similar cloud point values have been reported previously for a number of linear thermosensitive polymers (Magnusson et al., 2008). Hence, Poly(PEGMA188-ME-co-PEGMA475-ME) and Poly(PEGMA246-EE-co-PEGMA475-ME) were suitable for drug loading and its nasal delivery.

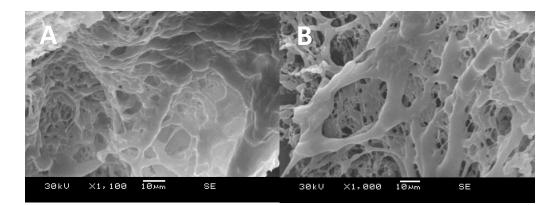**Fig. 1.** Cloud point measurements of polymers using UV−visible turbidimetry experiments at 550 nm in water (1 mg/mL) versus temperature.

3.4 SEM imaging

483 Fig. 2 depicts typical SEM micrographs of freeze-dried Poly(PEGMA188-ME-co-PEGMA475-
484 ME) and Poly(PEGMA246-EE-coPEGMA475-ME) hydrogels the microstructure of the interior
485 of the freeze-dried hydrogels was revealed. Poly(PEGMA188-ME-coPEGMA475-ME) hydrogels
486 had relatively regular pores of tens to hundreds of micrometres in size formed through well-
487 connected gel matrices.

488 The morphology of Poly(PEGMA246-EE-co-PEGMA475-ME) appeared somewhat different,
489 where an irregular, entangled fibrous morphology is noticed. It is obvious that gel matrices
490 appeared porous with channels/voids of 5–20 µm. Calculations indicated that this void volume
491 was equivalent to 60–75% porosity in the gels studied.

492 The porous network structure of these hydrogels with their biodegradability and relatively strong
493 gel strength suggested that these materials might be useful as drug delivery biomaterials the high
494 internal surface areas with low diffusional resistance would be favorable for small drug molecules
495 like RS to move freely in the polymeric network.

497 **Fig. 2.** Representative Scanning Electron Micrograph of (a) F2 and (b) F4.

499 **3.5. Incorporation of RS in thermoresponsive gels and pH determination**

500 Based on a preliminary study, the co-polymer solutions (Poly(PEGMA188-ME-coPEGMA475-
501 ME) and Poly(PEGMA246-EE-coPEGMA475-ME)) at 30% were chosen, owing to their
502 capability to form hydrogels upon heating in a water bath at 37°C. The developed in situ gels were
503 loaded with RS (0.2% w/v) by simple mixing (F2 and F4 respectively). The image of pre-gelled
504 solution and formed hydrogel are shown in Fig. 3.

505 The pH of nasal formulations should be such that the formulation will be stable at that pH and at
506 the same time there would be no irritation to the patient upon administration. Tolerable non-

507 irritable nasal formulations should have pH range in between 4.5 to 6.5. The pH values of

508 hydrogels were found to be within the physiologic range of nasal application amounting of 5.55 ±

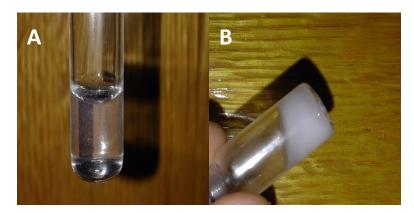509 0.02 and 5.79 ± 0.04 for F2 and F4, respectively.

510

511

512

513 **Fig. 3.** Sol-gel phase transitions of F2 in (a) a sol state at 25 °C, (b) gel state at 37 °C.

514

515

516 **3.6 Viscosity determination of RS loaded thermoresponsive gels**

517 Concerning rheological measurements, the rheograms obtained for the two investigated gels at

518 37°C displayed the pseudoplastic and shear-thinning behaviour (Fig. 4). Such rheological patterns

519 could therefore be preferred so that the viscosity decreases, facilitating the flow of the in-situ gel

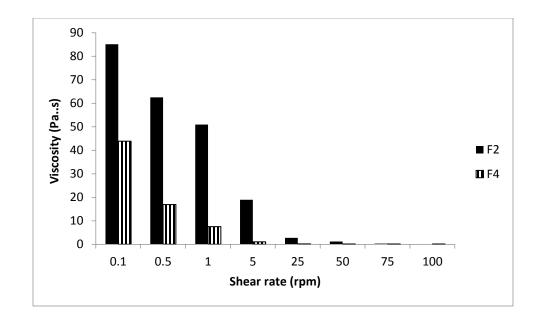520 upon application for intranasal use.

521

Fig. 4. Viscosity measurements of the investigated gel formulations. Data are reported as the mean of three independent experiments.

3.7 Bioadhesion strength of RS loaded thermoresponsive gels

When considering nasal delivery, it is highly desirable to formulate bioadhesive delivery vehicles to enhance their localization and retention time in the nasal area, thus intensifying the contact with nasal mucosa for the drug absorption. This was the basis for investigating the mucoadhesive properties for the prepared formulae in this study. The viscosity of the prepared formulae plays an important role in determining the mucoadhesive properties (Suvannasara et al., 2013). Therefore, in this work, mucoadhesive force between the interacting polymers (F2 and F4) and the mucin were elucidated based on viscosity data.

The results indicated rheological synergism and promising mucin-thermoresponsive gels association. The viscosity values of mucin-gels mixtures showed values of 1.85 ± 0.07 and 1.64 ± 0.016 Pa·s for F2 and F4 respectively. Such values were revealed to be higher than the sum of the corresponding viscosity values of the separate components of mucin (1.14 ± 0.11 Pa·s) and individual co-polymers (respective 0.10 ± 0.04 and 0.096 ± 0.008 Pa·s values for Poly(PEGMA188-ME-co-PEGMA475-ME) and Poly(PEGMA246-EE-co-PEGMA475-ME). Furthermore, F2 exhibited a significantly higher component of mucoadhesion (0.6 Pa·s), almost 1.51fold higher than that for F4 (0.39 Pa·s) (P<0.001). Therefore, such formulations were considered potential mucoadhesive intranasal drug delivery systems.

543 It was found that incorporating high molecular weight PEG based polymers onto the surfaces of
544 hydrogels and hydrogel microparticles enhanced mucoadhesion. PEG chains are able to
545 interpenetrate and associate with mucin by forming hydrogen bonds with its carbohydrate regions
546 hence acting as a 'glue' (Wang et al., 2008) (Maisel et al., 2016).

547

548 **3.8 In vitro drug release**

549 RS was utilized as a hydrophilic model drug to evaluate the feasibility of F2 and F4 for its sustained
550 delivery. RS has a log octanol/water partition-coefficient of -3.48 (Biernacka et al., 2013). Free
551 RS reached 100% release within 4 hours owing to its high polarity and hydrophilicity, similar to
552 that previously reported (Nasr et al., 2011). The release profile of RS from hydrogels is
553 investigated as shown in Fig. 5. The data indicates that 63 and 61.5 % of RS was released in 2 days
554 for F2 and F4 respectively under sink conditions. Such similar percent RS release was confirmed
555 by similarity factor calculated value ($f_2 = 72.37$).

556 RS exhibited an initial burst release from both hydrogel matrices reaching values of 43.7 and 37
557 % at first hour respectively followed by slowed and sustained release rate till the end of
558 experiment. The burst release of RS release was more likely due to the presences of RS on the
559 surface or distributed in the hydrogels network during the gelation process. Besides, the
560 hydrophilic RS might possess a higher tendency to partition in the hydrophilic domain of the
561 hydrogel and to diffuse rapidly and easily through the hydrogel into the release medium. The
562 porous network of the prepared matrices, observed in SEM images, confirmed the previous
563 hypothesis, indicating the diffusion-controlled drug release.

564 After that, the entrapped RS into the hydrogel was released slowly due to the swelling and
565 degradation of the hydrogel. Because the hydrogel did not degrade completely during the time of
566 investigation, some part of the RS entrapped in the inner core of the hydrogel would not be released
567 until the hydrogel was degraded entirely.

568 It is worthy to note that the prepared hydrogels (F2 and F4) exhibited a wide range of erosion rates
569 and maintained their mass for over two days. The percentage of gels that remained after 2 days
570 was 25 and 30% for F2 and F4, respectively (data not shown). F4 showed significantly higher
571 resistance against mass erosion in aqueous solution as compared to F2. This might be attributed to
572 its content of the longer chain length of PEGMA246-EE. Higher viscosity of the in situ platform

might also slow the degradation. Consequently, such in situ gels seemed to be more functional for a sustained RS delivery.

A similar release profile was observed for an intranasal thermosensitive hydrogel utilizing quaternized chitosan and poly(ethylene glycol) (Wu et al., 2007). Such a biphasic release pattern was a common finding seen in previous research papers studying the release of different biopharmaceuticals from thermosensitive hydrogels (Rangabhatla et al., 2016; Wu et al., 2007).

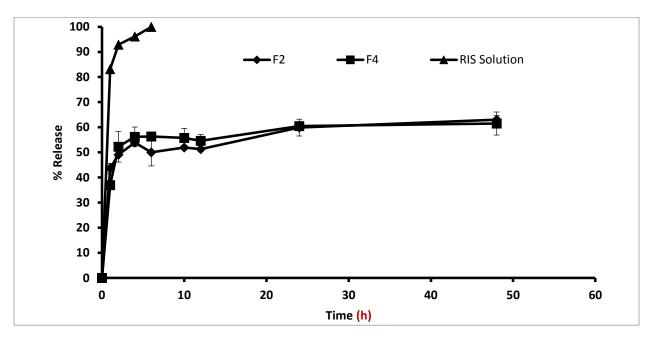**Fig. 5.** In vitro release profiles of RS and RS loaded gel formulations over 48 h. Data are reported as the mean ± S.D. of three independent experiments.

3.9. Ex-vivo permeation

Fig. 6 illustrates the amount of RS permeated per unit surface area of the sheep nasal mucosa versus time for F2 and F4, using RS solution as a comparison. RS-loaded formulae exhibited higher permeation as compared to RS solution. According to the biopharmaceutics classification system, RS belongs to class III (high solubility/low permeability) (Fazil et al., 2016; Jung and Han, 2014).

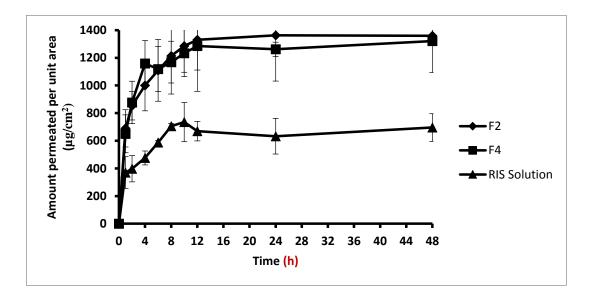Permeation enhancement potential of the two investigated formulations could be due to the surfactant properties of PEG ethers in the polymers (Casiraghi et al., 2015), possibly solving the permeability problem and low flux of RS (Nam et al., 2011). Additionally, the hydrogels took

more time for degradation in the biological system which showed permeation over 48 h. Moreover, the mucoadhesive capability of the thermogels might contribute to nasal retention which plays a very important role in transnasal penetration promoting effects.

The flux for F2 and F4 was found to be 70.9 and 94 $\mu g/cm^2h^{-1}$, respectively, while only flux value of 43.52 $\mu g/cm^2h^{-1}$ was depicted for RS solution, proving that the RS containing formulae possessed high penetration through the nasal mucosa. Similar to what was obtained in the in vitro release experiment, there was no statistically significant difference between the cumulative amount of RS from F2 and F4 permeated after 48 h ($p > 0.05$) (Maisel et al., 2016).

Fig. 6. Ex vivo permeation of RS from its solution and RS loaded gel formulations. Data are reported as the mean ± S.D. of three independent experiments.

3.10 In vivo study

Table 2. Biochemical analysis of serum levels of bone turnover markers for the different treatment groups. Data are reported as the mean ± S.D. of four independent experiments.

Experimental Group	Treatment	ALP (IU/l)	Serum Calcium (Ca) (mg/dl)	Serum Phosphorus (P) (mg/dl)	Serum creatinine (mg/dl)
Group I	IN saline	144.5±23.3	9.7±0.07	8.2±0.3	0.3±0.05

Group II	SC DEX	383±111.7	8.6±0.2	3.7±3.3	0.5±0.07
Group III	DEX+IN RS	304.5±3.5	9.8±0.4	8.9±1.6	0.3±0.05
Group IV	DEX+IV RS	217±125.9	9.9±0.3	9.4±2.4	0.3±0.26
Group V	DEX+IN F2	206±62.2	10.1±0.4	9±1.4	0.3±0.05
Group V1	DEX+IN F4	271±145.7	9.8±0.1	9.2±1.6	0.4±0.05

In this study, an osteoporosis model was induced by SC administration of toxic doses of dexamethasone sodium phosphate (DEX) in experimental rats. DEX, as a glucocorticoid, has the potential to compromise the skeletal integrity, decrease osteoblastic activity and promote osteoblast and osteocyte apoptosis, resulting in increased fractures risk and augmented bone loss (O'Brien et al., 2004; Yao et al., 2008).

Following induction of osteoporosis and RS treatment, biochemical markers, namely, alkaline phosphatase (ALP), calcium, inorganic phosphorus and creatinine, were tested. Serum ALP is an osteoblast-related protein that directly promotes osteoid formation and mineralization. It is a bone formation marker that used to indicate metabolic bone disease (Garnero and Delmas, 1993; Regidor et al., 2008). Serum calcium and phosphorus are also markers of osteoporotic bone and bone mineral content and creatinine is a marker of Bone resorption (Fazil et al., 2016).

Table 2 depicts the biochemical examination of serum levels of bone turnover markers. Group-I, which acted as a negative control, exhibited normal serum levels of ALP and creatinine amounting to 144.5 ± 23.3 (IU/l)) and 0.3 ± 0.05 (md/dl) respectively. On the other hand, the toxic group II, receiving SC DEX alone, showed a marked elevation in the serum levels of ALP and creatinine with respective values of 383 ± 111.7 (IU/l) and 0.5 ± 0.07 (mg/dl), the highest among all the tested groups, confirming the induction of GIO.

This was reversed by RS in all RS treated groups (groups III-VI). A significant reduction in ALP and creatinine serum levels below the toxic level were demonstrated confirming promising recovery and capability of decreasing GIO risk. A notable significant increase of these values was obtained as compared to those of normal group (group I) ($p<0.05$).

Concerning serum calcium and phosphorus levels, the toxic group exhibited significantly reduced values among all the tested groups, proving osteoporosis formation. Following induction of osteoporosis, fragile conditions of the bone led to the release of calcium and phosphorus and their urinary excretion and hence, their reduced absorption (Fazil et al., 2016). All treated groups with

636 different forms of RIS showed higher calcium and phosphorus levels, proving the ability of RS to

637 enhance the absorption of calcium and its bone deposition and to prevent bone-breaking tendency.

638

639 **3.11 Histopathological examination**

640 Histopathological examination of bones of animals of group I (normal control) (Fig. 7a) showed

641 no histopathological alteration and the normal histological structure of the osteoblasts. The toxic

642 group II histological manifestations exhibited focal areas of resorption with appearance of cavities

643 and multiple osteoclasts as indicated by white arrows (Fig.7b), confirming osteoporosis induction.

644 There were focal areas of resorption with few osteoclasts noticed in histological features in rats of

645 group III treated with IN solution. The histopathology of bone was quite similar to the picture in

646 rats of group IV, treated with IV solution, exhibiting focal area of osteogenesis with remodeling

647 of the osteoblasts (Fig.7 c and d).

648 As for rats of group V treated with F2, there were focal area of osteogenesis with osteoblasts

649 remodeling as well as formation of dark basophilic lines of bone deposition as indicated by black

650 arrows. The histopathological picture mirrored the results of treatment of osteoporosis (Fig.7e).

651 Group VI treated with F4 shows the ultimate treatment as manifested by the angiogenesis of newly

652 blood capillaries with dark basophilic line of bone deposition as indicated by white star. In

653 addition, osteoblasts arrangement was recorded (Fig.7f), achieving promising recovery following

654 osteoporosis induction.

655 The prepared in situ gels were superior in their inhibitory effect as compared to IN and IV

656 solutions, possibly due to proven low permeability of the hydrophilic drug. In addition, as for IN

657 solution, the expected rapid wash out owing to nasal mucociliary clearance might contribute to its

658 lower antiosteoporotic capability (Fazil et al., 2016).
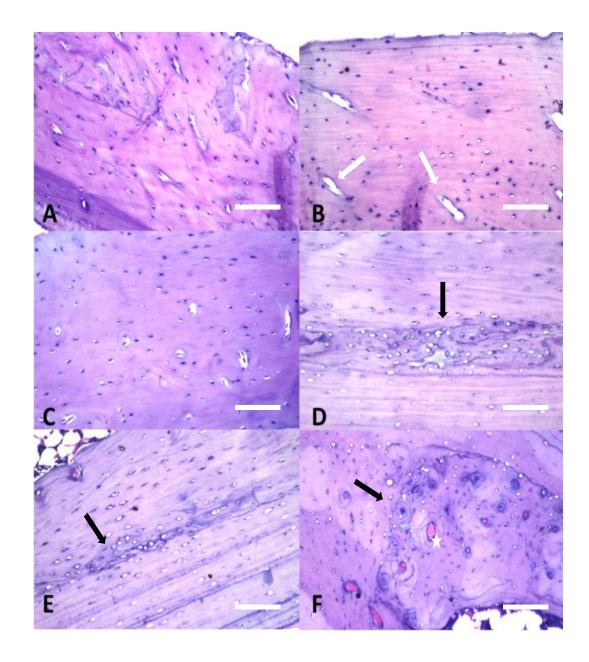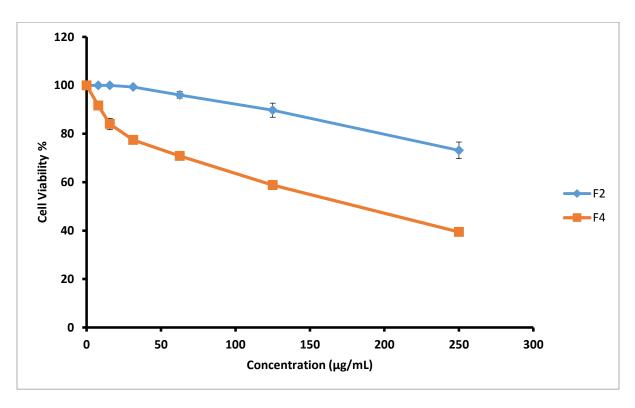
659

Fig.7. Light micrograph of rat internal structure of bone treated with (a) IN saline, (b) SC DEX, (c) DEX+IN RS, (d) DEX+IV RS, (e) DEX+F2 and (f) DEX+F4. White arrows indicate focal areas of resorption with appearance of cavities, black arrows indicate focal area of osteogenesis and white star indicates angiogenesis of newly blood capillaries (White bar 100 µm).

3.12 Evaluation of nasal cytocompatability

Mucoadhesive thermoresponsive hydrogels must be capable of delivering drugs in a sustained manner without compromising the host cell viability following nasal administration. In this regard, the effect of the prepared hydrogels on the cell viability of Calu-3 cells was investigated. Good cytocompatability was observed for F2 and F4 with no apparent cytotoxicity against the tested cells (cell viability >75%) after 24-h incubation at concentrations up to 250 and 62.5 µg/mL respectively (Fig. 8). It was only at hydrogel concentrations of 125 and 250 µg/mL that the cytotoxicity of F4 was significantly reduced. Lower cytocompatability values seen with F4 could be associated with its content of longer chains of PEGMA246-EE, possibly greatly interfering with the cell viability. Such values were comparable with other PEGMA-bearing copolymers utilized recently for drug delivery (Blanco-Fernandez et al., 2017). In addition, nonlinear PEG analogues had not induced cell death, even at a concentration as high as 10 mg /mL (Lutz, 2008).

Fig. 8. Viability of Calu-3 cells by MTT assay after incubation with various concentrations of the test samples at 37 °C. Data are reported as the mean ± S.D. of three independent experiments.

4. Conclusion

We suggest that the developed thermoresponsive in situ gels can contribute to the successful nasal delivery of RS. The characterization of the prepared in situ gels and the results of release, ex-vivo permeation experiments showed favourable rheological properties, mucoadhesive potential, sustained drug release and good permeability enhancement. Non-irritating pH value and cytocompatability of in situ gels confirmed their reasonable nasal tolerability. Moreover, better in vivo inhibitory effect of RS-loaded in situ gels was achieved compared to IN and IV RS solutions on osteoporosis induction in experimental rats. Hence, these newly developed in situ gel formulations have characteristics which are appropriate for mucoadhesive thermoresponsive delivery systems.

5. Acknowledgment

6. References

Alava, C., Saunders, B.R., 2006. Polymer stabilisers for temperature-induced dispersion gelation: Versatility and control. Journal of colloid and interface science 293, 93-100.

Aloorkar, N., Kulkarni, A., Patil, R., Ingale, D., 2012. Star polymers: an overview. Int. J. Pharm. Sci. Nanotechnol 5, 1675-1684.

Badi, N., Lutz, J.-F., 2009. PEG-based thermogels: applicability in physiological media. Journal of Controlled Release 140, 224-229.

Banchroft, J.D.S., A. And Turner, D.R., 1996. Fourth Ed. Churchil Livingstone, New York, London, San Francisco, Tokyo., Fourth Ed. Churchil Livingstone, New York, London, San Francisco, Tokyo.

Biernacka, J., Betlejewska-Kielak, K., Kłosińska-Szmurło, E., Pluciński, F., Mazurek, A.P., 2013. Prediction of bioavailability of selected bisphosphonates using in silico methods towards categorization into a biopharmaceutical classification system. Acta poloniae pharmaceutica 70, 877-882.

Blanco-Fernandez, B., Concheiro, A., Makwana, H., Fernandez-Trillo, F., Alexander, C., Alvarez-Lorenzo, C., 2017. Dually sensitive dextran-based micelles for methotrexate delivery. RSC Advances 7, 14448-14460.

Cai, Z., Song, X., Sun, F., Yang, Z., Hou, S., Liu, Z., 2011. Formulation and evaluation of in situ gelling systems for intranasal administration of gastrodin. AAPS PharmSciTech 12, 1102-1109.

Caló, E., Khutoryanskiy, V.V., 2015. Biomedical applications of hydrogels: A review of patents and commercial products. European Polymer Journal 65, 252-267.

Casiraghi, A., Selmin, F., Minghetti, P., Cilurzo, F., Montanari, L., 2015. Nonionic Surfactants: Polyethylene Glycol (PEG) Ethers and Fatty Acid Esters as Penetration Enhancers, Percutaneous Penetration Enhancers Chemical Methods in Penetration Enhancement. Springer, pp. 251-271.

Cespi, M., Bonacucina, G., Pucciarelli, S., Cocci, P., Perinelli, D.R., Casettari, L., Illum, L., Palmieri, G.F., Palermo, F.A. Mosconi, G., 2014. Evaluation of thermosensitive poloxamer 407 gel systems for the sustained release of estradiol in a fish model. European Journal of Pharmaceutics and Biopharmaceutics 88, 3, 954-961.

Chen, Z., Meng, H., Xing, G., Chen, C., Zhao, Y., Jia, G., Wang, T., Yuan, H., Ye, C., Zhao, F., 2006. Acute toxicological effects of copper nanoparticles in vivo. Toxicology letters 163, 109-120.

Czuryszkiewicz, T., Areva, S., Honkanen, M., Lindén, M., 2005. Synthesis of sol–gel silica materials providing a slow release of biphosphonate. Colloids and Surfaces A: Physicochemical and Engineering Aspects 254, 69-74.

Daoud, M., Cotton, J., 1982. Star shaped polymers: a model for the conformation and its concentration dependence. Journal de Physique 43, 531-538.

Dong, R., Zhou, Y., Huang, X., Zhu, X., Lu, Y., Shen, J., 2015. Functional supramolecular polymers for biomedical applications. Advanced materials 27, 498-526.

Fazil, M., Hassan, M.Q., Baboota, S., Ali, J., 2016. Biodegradable intranasal nanoparticulate drug delivery system of risedronate sodium for osteoporosis. Drug delivery 23, 2428-2438.

Fujita, Y., Watanabe, K., Uchikanbori, S., Maki, K., 2011. Effects of risedronate on cortical and trabecular bone of the mandible in glucocorticoid-treated growing rats. American Journal of Orthodontics and Dentofacial Orthopedics 139, e267-e277.

Galgatte, U.C., Kumbhar, A.B., Chaudhari, P.D., 2014. Development of in situ gel for nasal delivery: design, optimization, in vitro and in vivo evaluation. Drug delivery 21, 62-73.

Garnero, P., Delmas, P.D., 1993. Assessment of the serum levels of bone alkaline phosphatase with a new immunoradiometric assay in patients with metabolic bone disease. The Journal of Clinical Endocrinology & Metabolism 77, 1046-1053.

Gasteier, P., Reska, A., Schulte, P., Salber, J., Offenhäusser, A., Moeller, M., Groll, J., 2007. Surface Grafting of PEO-Based Star-Shaped Molecules for Bioanalytical and Biomedical Applications. Macromolecular bioscience 7, 1010-1023.

Harris, J.M., 2013. Poly (ethylene glycol) chemistry: biotechnical and biomedical applications. Springer Science & Business Media.

Hassan, E.E., Gallo, J.M., 1990. A simple rheological method for the in vitro assessment of mucin-polymer bioadhesive bond strength. Pharmaceutical research 7, 491-495.

Hirabayashi, H., Fujisaki, J., 2003. Bone-specific drug delivery systems. Clinical pharmacokinetics 42, 1319-1330.

Jeong, B., Kim, S.W., Bae, Y.H., 2012. Thermosensitive sol–gel reversible hydrogels. Advanced drug delivery reviews 64, 154-162.

Johnson, J.A., Baskin, J.M., Bertozzi, C.R., Koberstein, J.T., Turro, N.J., 2008. Copper-free click chemistry for the in situ crosslinking of photodegradable star polymers. Chemical Communications, 3064-3066.

Jung, I.-W., Han, H.-K., 2014. Effective mucoadhesive liposomal delivery system for risedronate: preparation and in vitro/in vivo characterization. International journal of nanomedicine 9, 2299.

799 Lapienis, G., 2009. Star-shaped polymers having PEO arms. Progress in Polymer Science 34, 852-
800 892.

801

802 Lee, T.Y., Roper, T.M., Jonsson, E.S., Kudyakov, I., Viswanathan, K., Nason, C., Guymon, C.,
803 Hoyle, C., 2003. The kinetics of vinyl acrylate photopolymerization. Polymer 44, 2859-2865.

804

805 Lietor-Santos, J., Kim, C., Lynch, M., Fernandez-Nieves, A., Weitz, D., 2009. The Role of
806 Polymer Polydispersity in Phase Separation and Gelation in Colloid− Polymer Mixtures. Langmuir
807 26, 3174-3178.

808

809 Liu, R., Fraylich, M., Saunders, B.R., 2009. Thermoresponsive copolymers: from fundamental
810 studies to applications. Colloid and Polymer Science 287, 627-643.

811

812 Loubat, C., Boutevin, B., 2001. Telomerization of acrylic acid with mercaptans: Part 2. Kinetics
813 of the synthesis of star-shaped macromolecules of acrylic acid. Polymer international 50, 375-380.

814

815 Lutz, J.F., 2011. Thermo-Switchable Materials Prepared Using the OEGMA-Platform. Advanced
816 Materials 23, 2237-2243.

817

818 Magnusson, J.P., Khan, A., Pasparakis, G., Saeed, A.O., Wang, W., Alexander, C., 2008. Ion-
819 sensitive "isothermal" responsive polymers prepared in water. Journal of the American Chemical
820 Society 130, 10852-10853.

821

822 Maisel, K., Reddy, M., Xu, Q., Chattopadhyay, S., Cone, R., Ensign, L.M., Hanes, J., 2016.
823 Nanoparticles coated with high molecular weight PEG penetrate mucus and provide uniform
824 vaginal and colorectal distribution in vivo. Nanomedicine 11, 1337-1343.

825

826 Moore, J.W., 1996. Mathematical comparison of dissolution profiles. Pharmaceutical technology
827 20, 64-75.

828

829 Nam, S.H., Xu, Y.J., Nam, H., Jin, G.-w., Jeong, Y., An, S., Park, J.-S., 2011. Ion pairs of
830 risedronate for transdermal delivery and enhanced permeation rate on hairless mouse skin.
831 International journal of pharmaceutics 419, 114-120.

832

833 Nancollas, G., Tang, R., Phipps, R., Henneman, Z., Gulde, S., Wu, W., Mangood, A., Russell, R.,
834 Ebetino, F., 2006. Novel insights into actions of bisphosphonates on bone: differences in
835 interactions with hydroxyapatite. Bone 38, 617-627.

836

837 Nasr, M., Awad, G.A., Mansour, S., Taha, I., Al Shamy, A., Mortada, N.D., 2011. Different
838 modalities of NaCl osmogen in biodegradable microspheres for bone deposition of risedronate
839 sodium by alveolar targeting. European Journal of Pharmaceutics and Biopharmaceutics 79, 601-
840 611.

841

842 Nasr, M., Taha, I., Hathout, R.M., 2013. Suitability of liposomal carriers for systemic delivery of
843 risedronate using the pulmonary route. Drug delivery 20, 311-318.

844

845 O'Brien, J.L., Gornick, F., 1955. Chain transfer in the polymerization of methyl methacrylate. I.
846 transfer with monomer and thiols. The mechanism of the termination reaction at 60 1. Journal of
847 the American Chemical Society 77, 4757-4763.

849 O'Brien, C.A., Jia, D., Plotkin, L.I., Bellido, T., Powers, C.C., Stewart, S.A., Manolagas, S.C.,
850 Weinstein, R.S., 2004. Glucocorticoids Act Directly on Osteoblasts and Osteocytes to Induce Their
851 Apoptosis and Reduce Bone Formation and Strength. Endocrinology 145, 1835-1841.

853 Pardal, F., Lapinte, V., Robin, J.-J., 2009. Kinetics of cotelomerization of 3-(trimethoxysilyl)
854 propyl methacrylate and perfluorodecylacrylate. European Polymer Journal 45, 1198-1207.

856 Rangabhatla, A.S.L., Tantishaiyakul, V., Oungbho, K., Boonrat, O., 2016. Fabrication of pluronic
857 and methylcellulose for etidronate delivery and their application for osteogenesis. International
858 journal of pharmaceutics 499, 110-118.

860 Regidor, D.L., Kovesdy, C.P., Mehrotra, R., Rambod, M., Jing, J., McAllister, C.J., Van Wyck,
861 D., Kopple, J.D., Kalantar-Zadeh, K., 2008. Serum alkaline phosphatase predicts mortality among
862 maintenance hemodialysis patients. Journal of the American Society of Nephrology 19, 2193-
863 2203.

865 Riggs, B.L., Melton, L.J.r., 1995. The worldwide problem of osteoporosis: insights afforded by
866 epidemiology. Bone 17, S505-S511.

868 Saeed, A.O., Magnusson, J.P., Moradi, E., Soliman, M., Wang, W., Stolnik, S., Thurecht, K.J.,
869 Howdle, S.M., Alexander, C., 2011. Modular construction of multifunctional bioresponsive cell-
870 targeted nanoparticles for gene delivery. Bioconjugate chemistry 22, 156-168.

872 Salzano, G., Marra, M., Porru, M., Zappavigna, S., Abbruzzese, A., La Rotonda, M., Leonetti, C.,
873 Caraglia, M., De Rosa, G., 2011. Self-assembly nanoparticles for the delivery of bisphosphonates
874 into tumors. International journal of pharmaceutics 403, 292-297.

876 Suvannasara, P., Juntapram, K., Praphairaksit, N., Siralertmukul, K., Muangsin, N., 2013.
877 Mucoadhesive 4-carboxybenzenesulfonamide-chitosan with antibacterial properties.
878 Carbohydrate polymers 94, 244-252.

880 Toussaint, N.D., Elder, G.J., Kerr, P.G., 2009. Bisphosphonates in chronic kidney disease;
881 balancing potential benefits and adverse effects on bone and soft tissue. Clinical Journal of the
882 American Society of Nephrology 4, 221-233.

884 Wang, Y.Y., Lai, S.K., Suk, J.S., Pace, A., Cone, R., Hanes, J., 2008. Addressing the PEG
885 mucoadhesivity paradox to engineer nanoparticles that "slip" through the human mucus barrier.
886 Angewandte Chemie International Edition 47, 9726-9729.

888 Wavikar, P., Pai, R., Vavia, P., 2017. Nose to Brain Delivery of Rivastigmine by In Situ Gelling
889 Cationic Nanostructured Lipid Carriers: Enhanced Brain Distribution and Pharmacodynamics.
890 Journal of pharmaceutical sciences 106, 3613-3622.

891

892 Wu, J., Wei, W., Wang, L.-Y., Su, Z.-G., Ma, G.-H., 2007. A thermosensitive hydrogel based on
893 quaternized chitosan and poly (ethylene glycol) for nasal drug delivery system. Biomaterials 28,
894 2220-2232.
895 Yao, W., Cheng, Z., Busse, C., Pham, A., Nakamura, M.C., Lane, N.E., 2008. Glucocorticoid
896 excess in mice results in early activation of osteoclastogenesis and adipogenesis and prolonged
897 suppression of osteogenesis: a longitudinal study of gene expression in bone tissue from
898 glucocorticoid-treated mice. Arthritis & Rheumatology 58, 1674-1686.
899

900 Yuan, C.M., Di Silvestro, G., 1995. Effect of polyfunctional chain transfer agents on the molecular
901 weight distribution in free-radical polymerization, 3 Polymerization of methyl methacrylate in the
902 presence of polyfunctional chain transfer agents. Macromolecular Chemistry and Physics 196,
903 2905-2913.

904